JOURNAL OF GEOPHYSICAL RESEARCH, VOL. 99, NO. C12, PAGES 25,281–25,294, DECEMBER 15, 1994

The effect of sea ice on the solar energy budget in the atmosphere-sea ice-ocean system: A model study

Zhonghai Jin, Knut Stamnes, and W. F. Weeks
Geophysical Institute, University of Alaska, Fairbanks

Si-Chee Tsay
NASA Goddard Space Flight Center, Greenbelt, Maryland

Abstract. A coupled one-dimensional multilayer and multistream radiative transfer model has been developed and applied to the study of radiative interactions in the atmosphere, sea ice, and ocean system. The consistent solution of the radiative transfer equation in this coupled system automatically takes into account the refraction and reflection at the air-ice interface and allows flexibility in choice of stream numbers. The solar radiation spectrum (0.25 μm-4.0 μm) is divided into 24 spectral bands to account adequately for gaseous absorption in the atmosphere. The effects of ice property changes, including salinity and density variations, as well as of melt ponds and snow cover variations over the ice on the solar energy distribution in the entire system have been studied quantitatively. The results show that for bare ice it is the scattering, determined by air bubbles and brine pockets, in just a few centimeters of the top layer of the ice that plays the most important role in the solar energy absorption and partitioning in the entire system. Ice thickness is important to the energy distribution only when the ice is thin, while the absorption in the atmosphere is not sensitive to ice thickness variations, nor is the total absorption in the entire system once the ice thickness exceeds about 70 cm. The presence of clouds moderates all the sensitivities of the absorptive amounts in each layer to the variations in the ice properties and ice thickness. Comparisons with observational spectral albedo values for two simple ice types are also presented.

1. Introduction

Polar sea ice plays an important role in the global climate system. Solar radiation is the dominant energy component controlling the heat and mass balance of sea ice in the polar regions. The atmosphere, sea ice, and ocean interact both directly and indirectly with each other via radiative transfers of energy. The atmospheric structure, clouds, the sea ice state, and the seawater below the ice determine the solar radiative energy distribution throughout the system, as well as the radiative energy absorbed in the ice and transmitted into the ocean. Radiation absorbed within the sea ice can change the internal structure of the ice and consequently its optical properties. These changes result in an alteration of the radiative energy transmitted into the ocean and reflected back to the atmosphere, which, in turn, affects the stratification and circulation of the atmosphere and the ocean. These radiative interactions can also affect the sensible, latent, and conductive energy exchanges between the subsystems due to the variations in structure and state of each layer. Therefore to understand the interaction between the atmosphere, sea ice, and ocean, it is necessary to investigate factors that affect the disposition of the solar radiation within this coupled system, such as the amount of the solar radiative energy stored in the interior of the ice, transmitted into the ocean, and reflected back to the atmosphere, respectively.

Numerous theoretical and experimental studies have been carried out to investigate the absorption and scattering of solar radiation by sea ice [*Grenfell and Maykut*, 1977; *Grenfell*, 1979, 1991; *Buckley and Trodahl*, 1987] and the penetration of radiation into the ocean [*Perovich and Maykut*, 1990; *Maykut and Grenfell*, 1975]. Studies of the role of solar radiation in the heat and mass balance of sea ice [*Untersteiner*, 1961; *Langleben*, 1966; *Shine and Crane*, 1984] have shown the importance of solar radiative energy on sea ice decay. Results from thermodynamic models clearly indicate that the equilibrium sea ice thickness is very sensitive to the amount of solar radiation impinging on the upper ice surface and its absorption in the interior of the ice [*Maykut and Untersteiner*, 1971; *Semtner*, 1976; *Ebert and Curry*, 1993].

While the direct effects of the incoming solar radiation on the heat and mass balance of the ice are now well

Paper number 94JC02426.
0148-0227/94/94JC-02426$05.00

understood and fairly easy to treat in models, relatively little is known about the quantitative partitioning of the absorbed radiation among the atmosphere, sea ice, and ocean and the effects of the ice state and clouds on this partitioning of energy. The purpose of this paper is to study the radiative transfer process in the coupled atmosphere-sea ice-ocean system and to assess quantitatively how the physical properties of the ice affect the disposition and partitioning of the solar radiative energy within the atmosphere, the sea ice, and the ocean, within the various layers in the ice, and within the system as a whole. We will also investigate the effects of clouds, surface snow cover, and surface melt ponds on the absorption and distribution of solar energy in the coupled system. To do this, we have developed a coupled radiative transfer model for the system. The model rigorously takes into account over the whole solar spectrum the multiple scattering and absorption by atmospheric gases, clouds, snow, ice, and seawater, as well as by inclusions in sea ice. In this model each stratum is divided into a sufficient number of layers to adequately resolve variations in optical properties. The multistream solution adopted obtains accurate, self-consistent solutions of the radiative transfer equation for the entire system that satisfies appropriate boundary and layer interface conditions, including the reflection and refraction at the air-ice and air-water interfaces.

2. Model Description

2.1. Radiative Transfer

The discrete ordinate method [*Chandrasekhar*, 1960; *Stamnes et al.*, 1988] is used to solve the radiative transfer equation in the atmosphere, sea ice, and ocean system. For this coupled system the main difficulty in solving this equation is caused by the change in the refractive indices at the interface between air and ice or air and ocean. Here we focus on the radiative energy computation for which only fluxes (irradiances) are needed. Therefore we may start with the azimuthally averaged version of the equation that describes the transfer of monochromatic radiation at frequency ν [*Chandrasekhar*, 1960; *Stamnes*, 1986]

$$\mu \frac{dI_\nu(\tau_\nu,\mu)}{d\tau_\nu} = I_\nu(\tau_\nu,\mu) - \frac{a(\tau_\nu)}{4\pi}\int_{-1}^{1} p_\nu(\tau_\nu,\mu',\mu) \times I_\nu(\tau_\nu,\mu')d\mu' - Q_\nu(\tau_\nu,\mu) \quad (1)$$

where μ is the cosine of the polar angle; τ_ν, the optical depth; $I_\nu(\tau_\nu,\mu)$, the azimuthally averaged diffuse intensity or radiance; $a_\nu(\tau_\nu)$, the single scattering albedo; and $p_\nu(\tau_\nu,\mu',\mu)$, the scattering phase function. The second term on the right-hand side in (1) represents multiple scattering, while the third term, $Q_\nu(\tau_\nu,\mu)$, denotes the source which drives the radiative transfer process in the system. Because we will focus on solar radiation, the thermal source has not been taken into account here. Also, because we have invoked direct-diffuse splitting, (1) describes only the diffuse radiation, and $Q_\nu(\tau_\nu,\mu)$ is the solar pseudosource. Thus the source term is due entirely to the solar radiation incident at the top of atmosphere. In the atmosphere it can be expressed as [*Jin and Stamnes*, 1994]

$$Q_\nu^{\text{air}}(\tau_\nu,\mu) = \frac{a_\nu(\tau_\nu)}{4\pi}F^s p_\nu(\tau_\nu,-\mu_0,\mu)\exp(-\tau_\nu/\mu_0) + \frac{a_\nu(\tau_\nu)}{4\pi}F^s R(-\mu_0,n)p_\nu(\tau_\nu,+\mu_0,\mu) \times \exp[-(2\tau_\nu^a-\tau_\nu)/\mu_0] \quad (2a)$$

while in the sea ice and ocean, it is

$$Q_\nu^{\text{ocn}}(\tau_\nu,\mu) = \frac{a_\nu(\tau_\nu)}{4\pi}\frac{\mu_0}{\mu_{0n}(\mu_0,n)}F^s T(-\mu_0,n) \times p_\nu(\tau_\nu,-\mu_{0n},\mu)\exp(-\tau_\nu^a/\mu_0) \times \exp[-(\tau-\tau_\nu^a)/\mu_{0n}]. \quad (2b)$$

Here F^s is the solar flux (irradiance) normal to the beam incident in direction $\theta_0 = \cos^{-1}\mu_0$ at the top of atmosphere, τ_ν^a is the total optical depth of the atmosphere, and $R(-\mu_0,n)$ and $T(-\mu_0,n)$ are, respectively, the reflectance and the transmittance of the solar beam at the interface of air and ice or air and ocean. Thus the first term on the right-hand side of (2a) represents the downward incident solar beam source, while the second term represents the upward beam source reflected back from the air-ice or air-water interface due to the change in the refractive index across the interface. The cosine of the refracted solar zenith angle in the ice and ocean, $\mu_{0n}(\mu_0,n)$, is related to μ_0 and the relative refractive index n by Snell's law

$$\mu_{0n}(\mu_0,n) = \sqrt{1-(1-\mu_0^2)/n^2}. \quad (3)$$

The method of solving (1), including the proper application of the interface and boundary conditions, has been described by *Jin and Stamnes* [1994]. We may write the solution for a layer in the atmosphere denoted by p as (omitting the subscript ν)

$$I_p(\tau,\mu_i^a) = \sum_{j=1}^{N_1}\{C_{-jp}G_{-jp}(\mu_i^a)\exp[-k_{jp}(\tau_p-\tau)] + C_{jp}G_{jp}(\mu_i^a)\exp[-k_{jp}(\tau-\tau_{p-1})]\} + Z_p^0(\mu_i^a)\exp(-\tau/\mu_0) + Z_p^{01}(\mu_i^a) \times \exp[-(2\tau^a-\tau)/\mu_0], \quad i=\pm1,\ldots,\pm N_1 \quad (4a)$$

and that for a layer in the sea ice and ocean denoted by p as

$$I_p(\tau,\mu_i^o) = \sum_{j=1}^{N_2}\{C_{-jp}G_{-jp}(\mu_i^o)\exp[-k_{jp}(\tau_p-\tau)] + C_{jp}G_{jp}(\mu_i^o)\exp[-k_{jp}(\tau-\tau_{p-1})]\} + Z_p^{02}(\mu_i^o)\exp[-\tau/\mu_{0n}(\mu_0,n)], \quad i=\pm1,\ldots,\pm N_2 \quad (4b)$$

where μ_i^a are the quadrature angles in the atmosphere, and μ_i^o are the quadrature angles in the ice and ocean.

The refraction between the sea ice and the ocean has been neglected, because with the ice above, most of the solar radiation reaching the ocean surface would be within the visible spectrum, where the indices of refraction of ice and water are similar. Thus quadrature angles for the ice and ocean are considered to be the same. N_1 and N_2 are the numbers of the discrete quadrature points (streams) applied when replacing the integral over angle in (1) by numerical quadrature. The terms k_{jp} and $G_{jp}(\mu_i)$ are the eigenvalues and eigenvectors, respectively, associated with the solution of the homogeneous version of (1) $[Q_\nu(\tau_\nu, \mu) = 0]$, whereas $Z_p^0(\mu_i^a)$, $Z_p^{01}(\mu_i^a)$, and $Z_p^{02}(\mu_i^o)$ are related to the particular solutions due to the source term $Q_\nu(\tau_\nu, \mu)$, and C_{jp} are coefficients to be determined from the interface and boundary conditions. To avoid exponential overflow, the scaling transformation as discussed by *Stamnes and Conklin* [1984] was used to obtain negative exponentials in (4a) and (4b). This scaling is also essential to avoid numerical ill-conditions when solving the linear equations required to obtain the constants of integration in the solution (the Cjp values).

Appropriate quadrature points (streams) and weights have been chosen for the interface continuity relations. To take into account the region of total reflection in the sea ice and ocean, separate angular quadrature points are adopted in addition to those used in the atmosphere and the refractive region of the sea ice and ocean. These quadratures are chosen so as to (1) simplify the implementation of the interface continuity condition, (2) automatically account for the refraction and reflection at the air-ice or air-water interface, (3) solve the radiative transfer equation in the coupled system consistently, and (4) avoid the loss of accuracy incurred by interpolation if the same number of streams are used in the atmosphere, sea ice, and ocean. The total number of quadrature points (streams) chosen for each stratum is flexible and is based on the optical properties and the accuracy required.

From the solutions of (1) the downward and upward fluxes (irradiances) $F_\nu^{\pm}(\tau_\nu)$ and the mean intensity $\bar{I}_\nu(\tau_\nu)$ (the total scalar irradiance divided by 4π in oceanographic terminology [*Morel and Smith*, 1982]) at optical depth τ_ν could be computed according to the following formulas [*Stamnes*, 1986]:

$$F_\nu^{\pm}(\tau_\nu) = 2\pi \int_0^1 \mu I_\nu(\tau_\nu, \pm\mu) d\mu = 2\pi \sum_{i=1}^{N} w_i \mu_i I_\nu(\tau_\nu, \pm\mu_i) \quad (5)$$

$$\bar{I}_\nu(\tau_\nu) = \frac{1}{2}\int_{-1}^{1} I_\nu(\tau_\nu, \mu) d\mu = \frac{1}{2} \sum_{\substack{i=-N \\ i\neq 0}}^{N} w_i I_\nu(\tau_\nu, \mu_i) \quad (6)$$

Since (5) and (6) are general formulas, when these are applied to actual computations, the quadrature number N, as well as the quadrature directions μ_i and weights w_i, are different in the atmosphere from those in the sea ice and ocean.

For the purpose of this paper we define the net flux (total irradiance) $F_\nu(\tau_\nu)$ and the flux divergence $dF_\nu(\tau_\nu)/dz$ at depth z as

$$F_\nu(\tau_\nu) = F_\nu{}^+(\tau_\nu) - F_\nu{}^-(\tau_\nu) \quad (7)$$

$$\frac{dF_\nu(\tau_\nu)}{dz} = 4\pi\alpha_\nu(z)\bar{I}_\nu(\tau_\nu) \quad (8)$$

where $\alpha_\nu(z)$ is the absorption coefficient. Thus in the absence of thermal emission sources the radiative flux divergence is equal to the absorption of solar radiation per unit volume at depth z. The integrations of (7) and (8) over frequency ν will produce the corresponding radiative quantities within the integrated spectral region.

2.2. Input Parameterizations

To compute the radiative quantities, we need to specify either the optical properties in every layer or the appropriate physical parameters from which one may derive the optical properties. In addition, we have to specify the bottom and top boundary conditions. The bottom boundary condition refers to the reflecting property of the bottom surface, i.e., the seafloor. As most areas of the polar oceans can be considered optically infinite in depth, the bottom boundary is not particularly important in this study, and assuming it to be a Lambertian surface is sufficient. The top boundary condition required is the incident solar spectrum and the solar elevation. The observational data describing the solar spectrum at the top of the atmosphere used here is from *Coulson* [1975].

Within the atmosphere we consider the absorption and scattering by atmospheric gases, clouds, and aerosols [*Tsay et al.*, 1989]. Although molecular (Rayleigh) scattering is dominated by nitrogen and oxygen gases which constitute more than 99% of the Earth's atmosphere, molecular absorption is dominated by trace gases, mainly water vapor, carbon dioxide, and ozone. The absorption by other minor trace gases is not considered in this study. To account for the total solar energy, one must integrate over the solar spectrum (0.25 μm-4.0 μm), a spectral region where numerous absorption lines exist [*Rothman et al.*, 1987]. As a result, incorporation of the line structures into a multiple-scattering radiative transfer code will result in a very time consuming computation. To maximize computational efficiency, parameterization of gaseous absorption over a spectral region containing many lines is necessary when absorption is included in a multiple-scattering scheme. Therefore the method called exponential-sum fitting of transmissions (ESFT) has been adopted.

The ESFT method approximates the transmission function of a given spectral region by a finite sum of M exponential terms as follows [*Hunt and Grant*, 1969; *Wiscombe and Evans*, 1977]:

$$T(u) = \sum_{i=1}^{M} w_i \exp(-b_i u) \quad (9)$$

where T represents the band transmission function and u denotes the equivalent absorber amount. The b_i are the equivalent absorption coefficients and the w_i are the associated weights. The $b_i u$ behave like monochromatic optical depths which can easily be incorporated into the multiple-scattering scheme. The main virtue of the ESFT method is that it reduces the nongray radiative transfer problem involving integration over a finite spectral interval (for which Beer's law does not apply) to a series of monochromatic problems. Also, the overlap of absorbing gases can be easily treated due to the multiplicative property of the transmission [*Goody and Yung*, 1989].

The optical properties of Arctic clouds are parameterized in terms of the equivalent radius RE and the liquid water content LWC of the cloud as follows [*Slingo*, 1989; *Tsay et al.*, 1989]:

$$a = c_1 + c_2 RE \tag{10a}$$

$$g = c_3 + c_4 RE \tag{10b}$$

$$\beta_{\text{ext}}/LWC = c_5 + c_6/RE \tag{10c}$$

where a, g, and β_{ext} are the single-scattering albedo, the asymmetry factor of scattering, and the extinction coefficient respectively. The c_i terms are parameterized coefficients determined from numerical fitting of these equations to the optical properties obtained by Mie computations [*Tsay et al.*, 1989].

The optical properties of snow, including possible soot contamination, are obtained through Mie computations, which require the refractive index of ice/soot and the mean radius of snow and soot particles as input. Here we have utilized the models of *Wiscombe and Warren* [1980] and *Warren and Wiscombe* [1980], whose results for computed snow albedo agree well with the available field measurements.

In sea ice the processes considered include the absorption by pure ice, scattering and absorption by brine pockets, and the solid salts trapped within the ice and scattering by air bubbles as described by *Grenfell* [1983, 1991]. To obtain the optical properties for the bulk ice, the relative amounts of each component in the sea ice have to be determined. Formulas developed by *Cox and Weeks* [1983], which calculate the volume fractions of brine, air, and solid salts present in the ice from the ice temperature, density and salinity, were used for this purpose. These relations show that the fractional volume of air is sensitive to bulk ice density, but not to ice salinity, while the fractional volume of brine is sensitive to the ice salinity and temperature, but not to the ice density. Therefore when the air volume, instead of ice density, is the directly available input parameter, the brine volume calculated from Cox and Weeks's formulation based on a approximated density should still be accurate enough.

The absorption coefficient for pure ice is based on the data sets reported by *Grenfell and Perovich* [1981] and *Warren* [1984]. The optical properties of the brine pockets, air bubbles, and solid salts are obtained from Mie calculations with assumed spherical shapes. Unfortunately, field observations on size distributions for these inclusions are few. Therefore we have assumed values that appear reasonable. The size distribution for air bubbles is represented by a power law [*Grenfell*, 1983], $N(r) = N_0 r^{-1.24}$, where the upper and lower limits of 2 mm and 0.1 mm were used. The solid salts are assumed to be monodisperse with radii of 10 μm. As might be expected, the solid salt contribution only becomes significant at ice temperatures below the crystallization temperature of $NaCl{\cdot}2H_2O$ (-22.9°C). Only one measurement on the size distribution of brine pockets has been reported by *Perovich and Gow* [1991] for young sea ice, but the lower and upper size limits and their relation with salinity and temperature were unknown. *Grenfell* [1991] assumed a constant number concentration of 10 per cubic millimeter and a monodisperse distribution. As this assumption could overestimate brine scattering if the salinity is low, we will assume a uniform size distribution with a number concentration of $0.6S$ per cubic millimeter (S is the salinity in per mil) to coincide with the observational brine pocket size (typically tenths of a millimeter). This size distribution also causes the rate of change of the radius with temperature to approximately agree with the correlation length change with temperature observed by *Perovich and Gow* [1991]. Owing to the large particle size and the anomalous scattering resulting from the similarity in the refractive indices of ice and brine, the phase functions of brine pockets always show an extremely strong forward scattering peak. Therefore most of the scattered light is concentrated in a very small cone around the forward direction and can be added back to the incident radiation, so that the actual scattering coefficient can be scaled down dramatically. In addition,

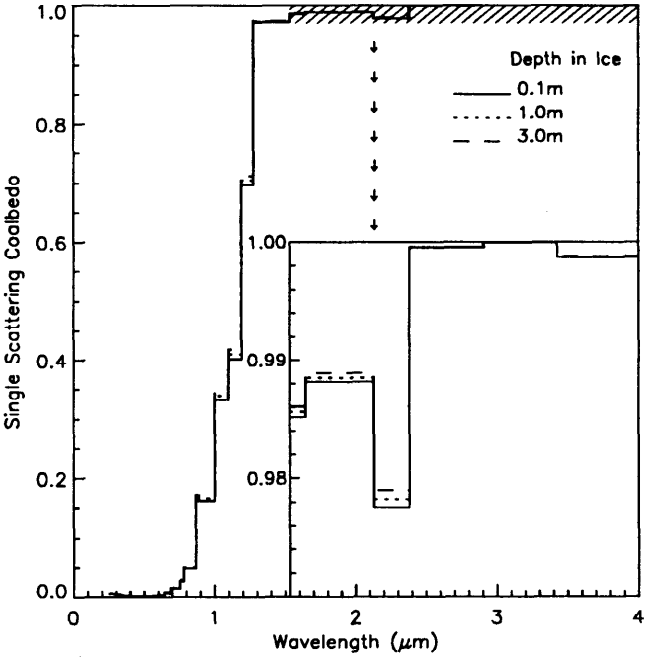

Figure 1. The single-scattering coalbedo at three levels for ice with thickness of 3.0 m, density of 0.9 Mg/m^3, salinity of 3‰ , and surface temperature of -10°C.

although an increase in brine pocket size will increase the extinction and scattering coefficients, this change will also strengthen the forward scattering, which actually reduces the scattering effectiveness. These factors make the error in radiation computation resulting from the uncertainty in brine size distribution much smaller than might be expected. As ice warms, the size distribution used here permits growth in the size of the brine pockets but ignores the merging of brine inclusions, which may decrease the scattering.

Each component in the sea ice interacts differently with radiation. Pure ice acts mainly as an absorber. Although air bubbles and brine pockets both scatter light strongly, air bubbles scatter more effectively, while brine pockets also absorb radiation. The optical properties of the sea ice depend on the volume occupied by each component.

In the ocean, scattering and absorption coefficients of seawater are taken from *Smith and Baker* [1981], who provide values applicable to the 0.2 μm to 0.8 μm region. For wavelengths larger than 0.8 μm, only absorption is considered, because the scattering is weak and the absorption is strong. We also neglect particulates in the ocean in this study, because of their minor effect on the energy budget in the coupled system.

3. The Radiative Energy Budget

For solar radiation the spectral region considered is from 0.25 μm to 4.0 μm, which includes approximately 99% of the total solar radiation energy incident at the top of the atmosphere. In this study the solar spectrum is divided into 24 bands and the ESFT method described earlier is adopted to simulate the absorption by water vapor, carbon dioxide, oxygen, and ozone in each band. For test purposes we have taken the profiles of pressure, gaseous concentrations in the atmosphere from the *McClatchey et al.* [1972] model atmosphere for the subarctic region and divided the atmosphere into 25 layers. For sea ice, although modeled salinity profiles

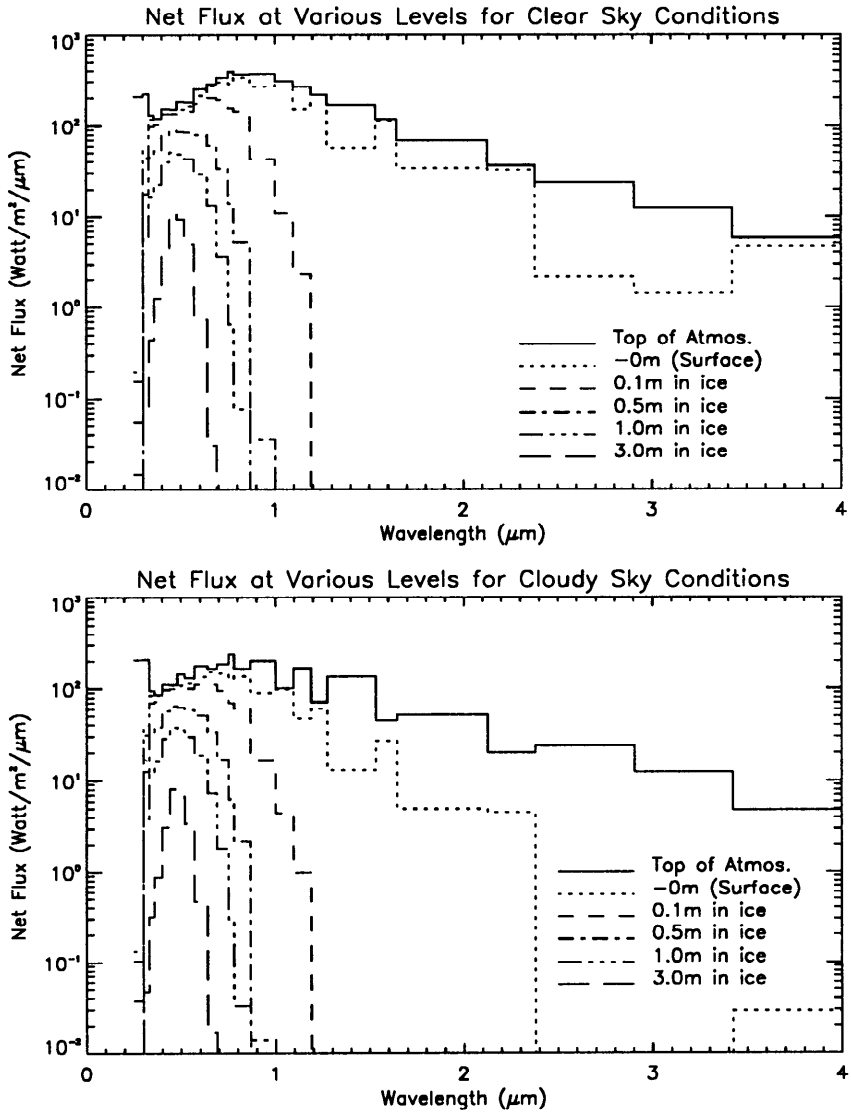

Figure 2. Spectral distribution of net flux at various levels for (top) clear sky and (bottom) cloudy sky conditions.

are available [*Cox and Weeks*, 1988; *Eicken*, 1992], an adequate treatment of density profile variations does not exist. Therefore, we will, as a first approximation, assume that although the density and salinity may change with thickness, for a given thickness these values are constant throughout the ice sheet. We will also assume that there is a linear temperature profile with the bottom temperature of the ice fixed at −2°C. Although this is known to be an excellent approximation for young ice types, as sea ice thickens, nonlinear effects become increasingly common [*Maykut*, 1978]. The ice is divided into three to seven layers in the following studies, depending on ice properties. In the ocean we will neglect vertical variations in the properties of seawater and consider it as one homogeneous layer.

3.1. Spectral Radiative Absorption

The first test is for ice with thickness 3.0 m, salinity $3‰$, density 0.90 Mg/m^3 and surface temperature −10°C, approximately the ice surface temperature in middle May and September observed in the central Arctic [*Maykut*, 1978]. For this ice model, which can be considered to be representative of multiyear ice, the single-scattering coalbedo (the ratio of the absorption coefficient and extinction coefficient) in the 24 spectral bands at three depths in the ice is shown in Figure 1, which indicates strong absorption in the infrared part of the solar spectrum and relatively weak absorption in the visible region. Figure 2 shows the net fluxes in the 24 spectral bands at various levels and with a solar zenith angle of 60°. The net (downward) flux is defined as the difference between the downward and upward fluxes (irradiances) as given by (7). Therefore the vertical distance between any two lines represents the radiation energy absorbed by a column with unit cross-sectional area between the corresponding two levels, and the area beneath the bottom line represents the absorption of radiation by the ocean. Figure 2 indicates that much of the solar radiation will be absorbed within the uppermost 0.1 m of the ice and the absorption also varies greatly as a function of wavelength, which is well correlated with the single-scattering coalbedo shown in Figure 1. Only the visible radiation can penetrate into the deeper layers of the ice and into the ocean.

For the same conditions as in Figure 2 (top) panel, but including a layer of Arctic stratus cloud in the atmosphere, Figure 2 (bottom) shows that the absorption by the atmosphere is increased, especially in the longer wavelength, due to the cloud absorption. Consequently, absorption by the ice and by the ocean will decrease in every spectral band, especially in the upper layer of the ice. On the basis of observational data [*Herman and Curry*, 1984; *Tsay and Jayaweera*, 1984], the cloud used here has an equivalent droplet radius of 7 μm and a water content of 0.2 g/m^3. The cloud base is assumed to occur at a height of 700 m with a thickness of 300 m, values typical for Arctic stratus.

3.2. Absorption and Partitioning of Solar Energy in the Atmosphere-Sea Ice-Ocean System

Next we use the same models for the atmosphere, cloud, sea ice, and ocean as in Figure 2, but change

Table 1. The Amount of Solar Energy Absorbed by Various Layers and Its Percentage of the Total for Different Ice Densities

Density, Mg/m^3	Total Absorption, W/m^2	Absorption in Various Layers and Its Percentage of the Total					
			Ice				
		Atmosphere	0-1 cm	1-10 cm	0.1-1 m	1-2 m	Ocean
		Visible (0.28 - 0.78 μm), Clear Sky					
0.86	62.6	21.4(34)	1.5(2.4)	10.4(17)	23.1(37)	3.1(4.9)	3.0(4.8)
0.88	73.2	21.1(29)	1.8(2.4)	12.5(17)	29.9(41)	3.3(4.5)	4.6(6.3)
0.90	90.5	20.8(23)	2.0(2.2)	14.7(16)	41.0(45)	4.4(4.9)	7.6(8.4)
0.92	127.7	20.0(16)	1.9(1.5)	16.0(13)	61.6(48)	9.7(7.6)	18.4(14.)
		Total (0.25 - 4.0 μm), Clear Sky					
0.86	315.1	114.9(36)	87.9(28)	72.2(23)	34.0(11)	3.1(1.0)	3.0(1.0)
0.88	334.5	114.3(34)	89.3(27)	79.5(24)	43.5(13)	3.3(1.0)	4.6(1.4)
0.90	361.8	113.5(31)	89.8(25)	86.8(24)	59.7(17)	4.4(1.2)	7.6(2.1)
0.92	411.6	112.2(27)	88.2(21)	90.8(22)	92.1(22)	9.8(2.4)	18.5(4.5)
		Visible (0.28 - 0.78 μm), Cloudy Sky					
0.86	50.4	21.5(43)	0.9(1.8)	6.7(13)	16.2(32)	2.5(5.0)	2.5(5.1)
0.88	56.3	21.3(38)	1.0(1.8)	7.6(14)	20.0(35)	2.6(4.5)	3.8(6.7)
0.90	65.2	21.1(32)	1.0(1.6)	8.2(13)	25.7(39)	3.2(4.9)	6.0(9.1)
0.92	81.4	20.8(26)	0.8(1.0)	7.4(9)	33.6(41)	5.9(7.2)	12.9(16.)
		Total (0.25 - 4.0 μm), Cloudy Sky					
0.86	210.2	132.9(63)	20.2(9.6)	30.8(15)	21.3(10)	2.5(1.2)	2.5(1.2)
0.88	217.7	132.6(61)	20.2(9.3)	32.5(15)	26.0(12)	2.6(1.2)	3.8(1.7)
0.90	228.3	132.2(58)	19.9(8.7)	33.5(15)	33.5(15)	3.2(1.4)	6.0(2.6)
0.92	246.3	131.7(53)	18.9(7.7)	31.2(13)	45.6(19)	5.9(2.4)	12.9(5.2)

Percentages of the total energy absorbed by different layers are given in parentheses.

the ice thickness to 2 m and the ice salinity to 5‰, values representative of average salinity for thick, first-year ice [*Cox and Weeks*, 1988]. Table 1 quantitatively shows the distribution of the absorbed radiative energy by the atmosphere, ocean and various sublayers of the ice under both clear and cloudy sky conditions for this situation. The values in the second column represent the total amount absorbed by the entire atmosphere-sea ice-ocean system. The total solar absorption is obtained by integration over the 24 spectral bands ranging from 0.25 μm to 4.0 μm, and the total visible absorption is the integral over 12 spectral bands ranging from 0.28 μm to 0.78 μm. The energy absorbed by different layers and its percentage of the total (values in the parentheses) are listed in the rest of the columns. The data in Table 1 show that the total disposition of the solar radiation in the entire atmosphere-sea ice-ocean system is sensitive to bulk ice density (i.e., the amount of air included in the ice). This is especially true for visible radiation, which experiences a twofold increase under clear sky conditions when the ice density increases from 0.86 Mg/m^3 to 0.92 Mg/m^3. However, the presence of a cloud drastically reduces this sensitivity to ice density. The cloud also reduces the total absorption in the coupled system, because the cloud reflects more solar radiation back to space. The total system albedo is increased from 0.53 under a clear sky to 0.69 under a cloudy sky for the cloud used here and for the ice density of 0.86 Mg/m^3 (from 0.46 to 0.67 for ice density 0.90 Mg/m^3). Although the total radiative absorption in the whole system increases with ice density, the percentage of absorption by the atmosphere decreases, and consequently the amount of absorption in the atmosphere remains almost unchanged. In fact, the atmospheric absorption decreases slightly with increasing ice density. The explanation for this is that less dense ice includes more air bubbles, which scatter and thereby reflect more radiation back to the atmosphere. Under clear sky conditions the top layer in the ice acts as a main absorber with the uppermost 1 cm of the ice absorbing more than 20% of the total radiative energy deposited in the whole atmosphere-sea ice-ocean system. Clouds significantly reduce both the amount and the percentage absorbed by the top layer of the ice, because most of the infrared part of the solar radiation has been absorbed and reflected by the cloud before it reaches the ice surface. Owing to less backscattering because of fewer air bubbles, denser ice also results in more transmission of radiation into the ocean and therefore produces higher absorption in the seawater under the ice. The sensitivity of this absorption by the ocean to the ice density is also reduced by clouds.

Similar to Table 1, Table 2 shows the partitioning of the absorbed solar radiation in the atmosphere-sea ice-ocean system for different ice salinities but with a fixed ice density of 0.9 Mg/m^3. These results show that the total absorption of solar radiation in the whole system decreases as the ice salinity increases and that this sensitivity is reduced by the presence of clouds. The atmosphere contributes more to the total radiative absorption as the ice salinity increases, because high salinity means more brine in the ice and therefore more brine

Table 2. The Amount of Solar Energy Absorbed by Various Layers and Its Percentage of the Total for Different Ice Salinities

Salinity, ‰	Total Absorption, W/m^2	Absorption in Various Layers and Its Percentage of the Total					
			Ice				
		Atmosphere	0-1 cm	1-10 cm	0.1-1 m	1-2 m	Ocean
		Visible (0.28 - 0.78 μm), Clear Sky					
2.0	114.9	20.5(18)	2.4(2.1)	19.1(17)	58.4(51)	7.6(6.6)	6.9(6.0)
6.0	84.0	20.9(25)	1.8(2.2)	13.2(16)	35.8(43)	5.5(6.5)	6.8(8.0)
10.0	73.9	21.3(29)	1.4(1.9)	10.1(14)	31.6(43)	6.0(8.2)	3.4(4.5)
14.0	71.9	21.4(30)	1.4(1.9)	9.5(13)	32.8(46)	5.9(8.1)	1.0(1.4)
		Total (0.25 - 4.0 μm), Clear Sky					
2.0	392.0	112.9(29)	93.0(24)	93.2(24)	78.3(20)	7.6(1.9)	6.9(1.8)
6.0	353.3	113.7(32)	88.7(25)	84.5(24)	54.1(15)	5.5(1.6)	6.8(1.9)
10.0	335.2	114.4(34)	85.0(25)	77.6(23)	48.8(15)	6.0(1.8)	3.4(1.0)
14.0	325.6	114.8(35)	82.1(25)	73.0(22)	48.8(15)	5.9(1.8)	1.0(0.3)
		Visible (0.28 - 0.78 μm), Cloudy Sky					
2.0	77.5	20.8(27)	1.3(1.7)	10.1(13)	35.2(45)	5.1(6.6)	4.9(6.3)
6.0	61.6	21.2(34)	0.9(1.5)	7.4(12)	22.5(37)	4.1(6.7)	5.4(8.7)
10.0	57.3	21.4(37)	0.8(1.4)	6.1(11)	21.6(38)	4.7(8.2)	2.7(4.7)
14.0	57.2	21.6(38)	0.8(1.4)	6.2(11)	23.3(41)	4.5(7.9)	0.8(1.4)
		Total (0.25 - 4.0 μm), Cloudy Sky					
2.0	241.5	131.9(55)	20.8(8.6)	35.4(15)	43.4(18)	5.1(2.1)	4.9(2.0)
6.0	224.4	132.3(59)	19.6(8.7)	32.6(15)	30.3(13)	4.1(1.8)	5.4(2.4)
10.0	218.7	132.7(61)	18.7(8.6)	30.8(14)	29.1(13)	4.7(2.1)	2.7(1.2)
14.0	217.2	133.0(61)	18.1(8.3)	30.2(14)	30.6(14)	4.5(2.1)	0.8(0.4)

Percentages of the total energy absorbed by different layers are given in parentheses.

pockets acting as scatterers, increasing the amount of reflected radiation. As the light propagates into the deeper layers of the ice and into the ocean, both the amount and the percentage of the radiative absorption in these layers do not show nearly as strong a dependence on the salinity as they did on the density, as was demonstrated in Table 1. This is due to the different scattering and absorptive properties of brine pockets and air bubbles. Brine pockets are stronger forward scatterers than the air bubbles, and, in addition, they also act as absorbing bodies.

Table 3 shows the distribution of the total solar radiation absorbed by the atmosphere, snow, ice, and ocean for different snow depths on the ice and for a fixed ice density (0.90 Mg/m^3) and salinity ($5‰$). The snow is specified to have a average grain radius of 1.0 mm and density of 0.4 Mg/m^3, values representative of old snow near the melting point [*Wiscombe and Warren*, 1980]. When the results in Table 3 are compared with those in Tables 1 and 2 for clear sky conditions, the total solar radiation disposition in the whole system is significantly reduced because of the higher reflection at the snow surface and the resulting isolation of the absorptive ice below. Although the absorption by snow and ice are different for different snow thicknesses, the total absorption by the whole system and the absorption by the atmosphere are similar for the four snow depths used, indicating the snow surface albedo is already saturated when the snow thickness exceeds 5 cm. Even more importantly, only 5 cm of snow layer is responsible for nearly half of the total solar absorption.

Similar to Table 3, Table 4 shows the partioning of the absorbed total solar radiation across the system obtained under four different solar elevations. As expected, a lower solar elevation (larger zenith angle) causes less absorption in the whole system, because it implies less radiative energy input to the system and also produces a higher reflection at the ice surface. Furthermore, for lower solar elevations, as a result of a higher reflection at the surface and a longer pathlength of light, a larger fraction of the total absorption occurs in the atmosphere and a correspondingly smaller fraction in the various layers of the ice and in the ocean. However, the presence of a cloud will increase the sensitivity of the fractional absorption in the ice and in the ocean to changes in solar elevation.

The occurrence of melt ponds on the ice has been shown to be important in the overall energy balance [*Ebert and Curry*, 1993]. A simulation of the solar energy distribution for different pond depths is presented in Table 5. Here we assumed that the pond depth is uniform, and we computed the energy distribution in a one-dimensional column of atmosphere, pond-over-ice, sea ice, and ocean but ignored interaction with neighboring columns. This treatment is mandated by our use of one-dimensional model. To simulate two-dimensional effects, one could, as a first approximation, use area-weighted combinations of different surface types as discussed for combination of leads and ice below. The same models for atmosphere, cloud, and ocean are used as above. Although the temperature at the ice top is 0°C and somewhat lower in the interior, for simplicity the temperature is specified to be −2°C (the same as the bottom temperature) throughout the complete ice thickness. The density is specified to be 0.93 Mg/m^3 when air volume is negligible, as it is for ice under ponds. A comparison with the results in the aforementioned tables shows that the total absorption by the whole system has been increased due to the reduced surface albedo. Also, the radiation penetration into the ocean has increased, while the absorption by the atmosphere shows only a slight change. A melt pond with a depth of only 5 cm can absorb nearly half of the total energy absorbed by the whole system.

The values in Tables 1, 2, and 4 indicate that although clouds reduce the total solar radiative absorption in the entire atmosphere-sea ice-ocean system, they can increase the amount of absorption in the atmosphere for the cloud model adopted here and consequently contribute to solar heating in the atmosphere. Although the increasing percentage and amount of solar absorption in the atmosphere due to the cloud is

Table 3. Absorbed Solar Energy by Various Layers and Its Percentage of the Total for Different Snow Depths

Snow Depth, cm	Total Absorption, W/m^2	Absorption in Various Layers and Its Percentage of the Total					
				Ice			
		Atmosphere	Snow	0-0.1 m	0.1-1 m	1-2 m	Ocean
				Clear Sky			
5	275.9	117.0(42)	130.5(47)	11.2(4.1)	13.3(4.8)	1.7(0.6)	2.2(0.8)
10	275.9	117.0(42)	142.2(51)	3.0(1.1)	10.2(3.7)	1.3(0.5)	2.2(0.8)
20	275.9	117.0(42)	147.9(54)	1.6(0.6)	6.4(2.3)	0.7(0.3)	2.2(0.8)
30	275.9	117.0(42)	152.2(55)	0.8(0.3)	3.4(1.2)	0.3(0.1)	2.2(0.8)
				Cloudy Sky			
5	200.2	133.7(67)	43.7(22)	7.9(4.0)	11.3(5.6)	1.5(0.8)	2.0(1.0)
10	200.2	133.7(67)	52.0(26)	2.4(1.2)	8.9(4.5)	1.1(0.6)	2.0(1.0)
20	200.2	133.7(67)	56.8(28)	1.4(0.7)	5.6(2.8)	0.7(0.3)	2.0(1.0)
30	200.2	133.7(67)	60.5(30)	0.7(0.4)	3.0(1.5)	0.3(0.2)	2.0(1.0)

Percentages of the total energy absorbed by different layers are given in parentheses.

Table 4. The Total Solar Energy Absorbed by Various Layers and Its Percentage of the Total for Different Solar Zenith Angles

Solar Zenith Angle, degree	Total Absorption, W/m^2	Absorption in Various Layers and Its Percentage of the Total					
			Ice				
		Atmosphere	0-1 cm	1-10 cm	0.1-1 m	1-2 m	Ocean
			Clear Sky				
40	573.7	158.1(28)	142.5(25)	147.8(26)	104.4(18)	7.7(1.3)	13.2(2.3)
60	361.8	113.5(31)	89.8(25)	86.8(24)	59.7(17)	4.4(1.2)	7.6(2.1)
70	235.5	84.7(36)	55.8(24)	52.1(22)	35.6(15)	2.7(1.1)	4.6(1.9)
80	105.6	50.4(48)	20.0(19)	19.0(18)	13.4(13)	1.0(1.0)	1.8(1.7)
			Cloudy Sky				
40	383.8	196.8(51)	39.4(10.)	65.1(17)	64.9(17)	6.1(1.6)	11.4(3.0)
60	228.3	132.2(58)	19.9(8.7)	33.5(15)	33.5(15)	3.2(1.4)	6.0(2.6)
70	148.0	93.5(63)	11.1(7.5)	19.0(13)	19.1(13)	1.8(1.2)	3.4(2.3)
80	72.3	51.4(71)	4.1(5.7)	7.2(10)	7.4(10)	0.7(1.0)	1.4(1.9)

Percentages of the total energy absorbed by different layers are given in parentheses.

strongly dependent on solar elevation (also on liquid water path and height of clouds, as our unpublished results show), it is insensitive to ice density and salinity. Results in Tables 1 and 2 show that in the deeper layers of the ice (depth H > 1.0 m) and in the ocean the total amount of absorbed solar energy is equal to the amount absorbed in the visible portion of the spectrum in these same layers. This clearly demonstrates that only visible radiation penetrates to these layers.

From these tables it is not difficult to determine the fraction of the net incoming solar radiation which penetrates into the interior of the ice (below a depth of 10 cm). This is an important parameter used in ice thermodynamic models [*Maykut and Untersteiner*, 1971; *Semtner*, 1976; *Ebert and Curry*, 1993] and polar climate models [*Parkinson and Washington*, 1979; *Bennett*, 1982; *Van Ypersele*, 1990]. For cloudy skies this value is dependent on the cloud conditions. For clear skies the tables show a minimum of 0.20, which corresponds to the lowest ice density (highest air volume) used in Table 1. This value is higher than values (typically 0.17 or 0.18) used in ice thermodynamic models and climate models, while the parameters for sea ice used in the tables should have covered most of the ice property variations. This value is primarily determined by the scattering properties of the air bubbles in the uppermost few centimeters of ice.

3.3. Radiative Heating in Sea Ice

To demonstrate how the absorption within the sea ice responds to the variation of the physical properties of the ice, Figure 3 shows the absorption profiles (heating rates), $dF(z)/dz$ (in milliwatts per cubic centimeter), with depth in the sea ice for different densities and salinities under clear sky conditions. Here z is the depth in the sea ice measured downward from the upper ice surface. The same model inputs for atmosphere, sea ice, and ocean as used in Figure 2 have been used in these computations. The thicker lines in the plots represent the total absorbed solar radiation (0.25 μm-4.0 μm) while the thinner lines represent the radiative energy absorbed in the visible region (0.28 μm-0.78 μm). Owing to the rapid decrease in radiative absorption with depth in the near-surface layer of the ice, logarithmic scales were chosen for both axes.

Table 5. Absorbed Solar Energy by Various Layers and Its Percentage of the Total for Different Depths of Melting Ponds

Pond Depth, cm	Total Absorption, W/m^2	Absorption in Various Layers and Its Percentage of the Total					
				Ice			
		Atmosphere	Ponds	0-0.1 m	0.1-1 m	1-2 m	Ocean
				Clear Sky			
5	408.9	112.2(27)	176.8(43)	40.7(9.9)	55.8(14)	7.7(1.9)	15.8(3.9)
10	418.8	111.9(27)	224.0(54)	18.9(4.5)	41.8(10)	6.7(1.6)	15.5(3.7)
20	432.7	111.6(26)	264.0(61)	9.2(2.1)	27.8(6)	5.2(1.2)	14.9(3.4)
40	450.3	111.2(25)	302.1(67)	3.9(0.9)	16.0(4)	3.2(0.7)	13.9(3.1)
				Cloudy Sky			
5	243.1	131.7(54)	48.7(20)	16.4(6.7)	29.9(12)	5.0(2.1)	11.3(4.7)
10	245.8	131.6(54)	67.0(27)	8.8(3.6)	23.1(9)	4.4(1.8)	11.0(4.5)
20	249.8	131.5(53)	84.0(34)	4.7(1.9)	15.9(6)	3.3(1.3)	10.4(4.2)
40	255.1	131.5(52)	100.4(39)	2.2(0.9)	9.5(4)	2.0(0.8)	9.5(3.7)

Percentages of the total energy absorbed by different layers are given in parentheses.

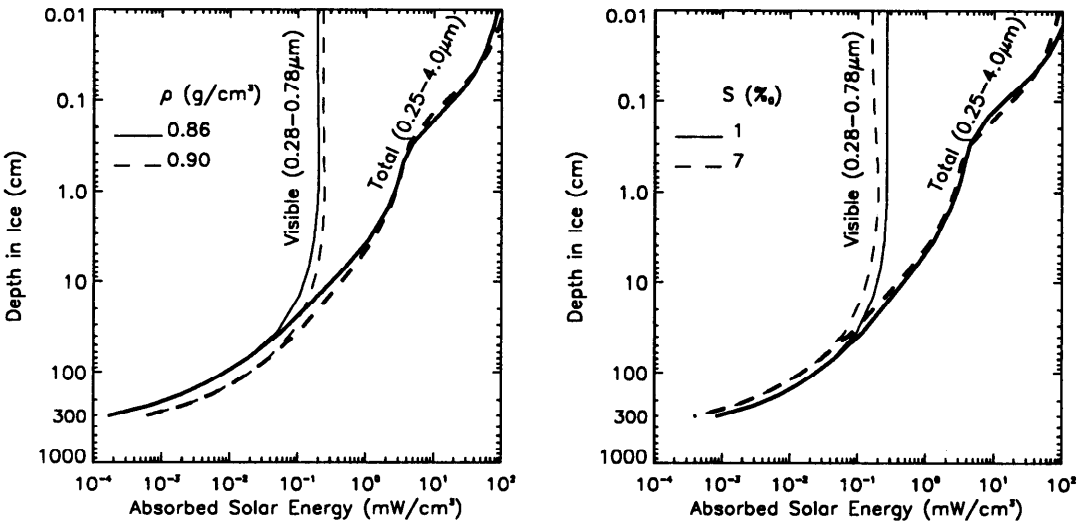

Figure 3. Distribution of the absorbed solar energy with depth in the ice for different (left) ice densities and (right) salinities under clear sky conditions.

These figures clearly demonstrate that although the absorption profiles are complicated within the first few centimeters of the top layer, below this depth, the radiative absorption increases as ice density increases and as salinity decreases. Again, these phenomena can be attributed to the different optical properties possessed by the different components in the ice. Generally, pure ice absorbs strongly in the whole solar spectrum except in the relatively narrow visible region, where a larger part of the solar radiative energy reaching the ice surface is concentrated. Both denser ice and less saline ice contain a larger fractional volume of pure ice, resulting in increased absorption. On the other hand, denser ice includes less air bubbles and the less saline ice includes less brine volume. Both of these reductions in the number of scatterers reduce the optical path for light propagating to deeper layers and consequently decrease the amount of absorption. Therefore the magnitude of the radiative absorption in the ice depends on these two competitive processes.

Most of the infrared and ultraviolet energy in the solar radiation reaching the ice surface would be absorbed within a very thin top layer of the ice because of the strong absorption by pure ice at those wavelengths. Consequently, in the upper layers of sea ice the absorption of the total solar radiation is dominated by the presence of pure ice. This is reflected in Figure 3 by the total solar radiative absorption in the thin top layer increasing as ice density increases and as salinity decreases. Then, as more infrared radiation has been absorbed, enhanced absorption due to multiple scattering becomes more important and dominates immediately beyond the thin top layer, causing an increase in the total solar absorption as the ice density decreases and the salinity increases. However, absorption below the depth of a few centimeters, where most of the remaining radiation is in the visible spectrum, will increase with increasing ice density and decreasing salinity due to the less scattering, leading to less reflection by the ice. The absorption rate in the visible spectrum shows only a small change within about 10 cm of the top layer. Figure 3 shows that the absorbed amounts of total radiation and visible radiation get closer and closer as the depth increases, and at about 50 cm in depth they overlap. This indicates that almost all the radiation beyond the visible region is absorbed by the top 50 cm of sea ice.

3.4. Effects of the Ice Thickness

In this example we will investigate the effects of the ice thickness on the radiative energy budget in the atmosphere-sea ice-ocean system using the same atmosphere, cloud, and ocean models as above. The ice model is also similar, but observed changes in the average salinity as a function of ice thickness are now included based on a recent compilation of first-year ice data by W. F. Weeks (personal data, 1994). The mean salinity values S are observed to be well described by the following two linear relations:

$$S = 17.0 - 31.63h_i, \qquad h_i \leq 0.3\,\text{m} \tag{11a}$$

$$S = 8.0 - 1.63h_i, \qquad h_i > 0.3\,\text{m} \tag{11b}$$

The temperature at the top of the ice will still be assumed to remain at $-10°C$ and to increase linearly with depth to $-2°C$ at the ice-water interface. Figure 4 shows the dependence of the total solar energy absorbed by the atmosphere, sea ice, and ocean, respectively, on the ice thickness. Results indicate that although the total solar energy disposed in the entire system decreases as ice thickness increases, the rate of decrease becomes smaller as the ice thickness increases, with the total radiative absorption approaching a nearly constant value after the ice thickness reaches about 70 cm. As the ice thickness increases, the absorption by the ice increases and that by the ocean decreases, with the rates of change, again, depending on the ice thickness. On the other hand, the absorption by the atmosphere remains almost unchanged as ice thickness changes. A comparison of the two panels in Figure 4 indicates that not

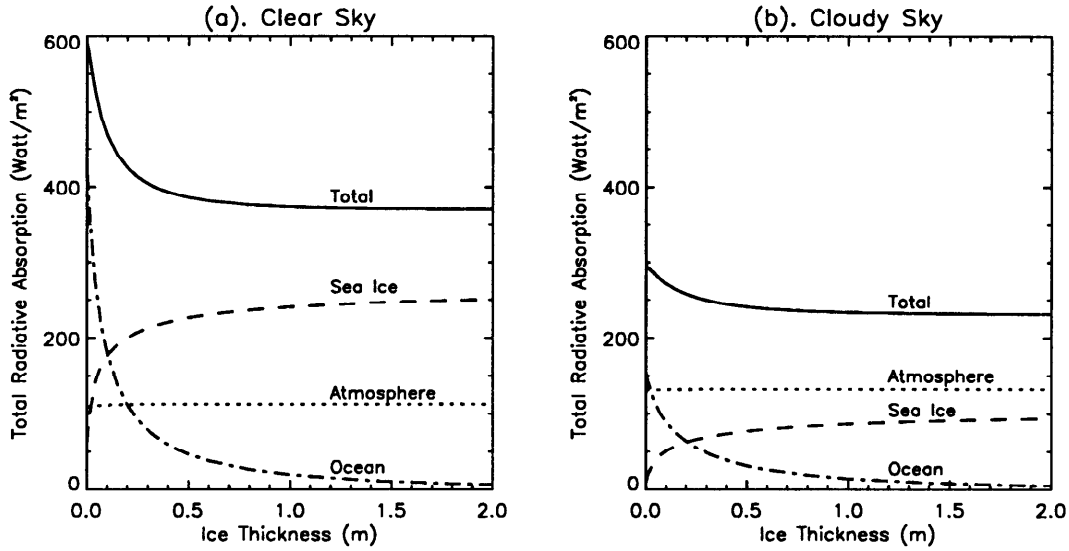

Figure 4. The distribution of total solar radiative absorption in the atmosphere, sea ice, and ocean system as a function of the ice thickness for (a) clear sky and (b) cloudy sky conditions.

only does the cloud drastically reduce the energy disposition into the ice and the whole system for any ice thickness and that into the ocean for thin ice, but also it significantly reduces all sensitivities of the absorbed solar energy to the ice thickness, especially when the ice is thin. The solar zenith angle used here is still at 60°. However, our unpublished results show that the general behavior indicated above is true for all solar elevations and cloud heights except that the magnitudes of all the components change.

3.5. Effects of Open Ocean

It is well known that the occurrence of areas of open water (leads, polynya) within an ice field has an important impact on the solar energy distribution. Using the same models as used in Tables 3 and 4, Figure 5 shows the solar energy partioning in the atmosphere, sea ice, and ocean (including open ocean and ocean under the ice) as a function of the area fraction of open water. The absorption by the atmosphere, ice, and ocean are represented by different shades of gray in Figure 5. Here the vertical distance covered by the three different shades gives the fraction of absorption. Area-weighted irradiances are used in this computation, as explained earlier. A similar method has been used and discussed by *Perovich* [1990] in estimating light reflection and transmission by spatially varying sea ice covers. This procedure actually ignores the horizontal radiation interaction by multiple scattering between the two different columns. Figure 5 shows that as the area fraction of open water increases, the solar radiation deposited in the ocean increases rapidly, from 2% under the ice cover to 80%

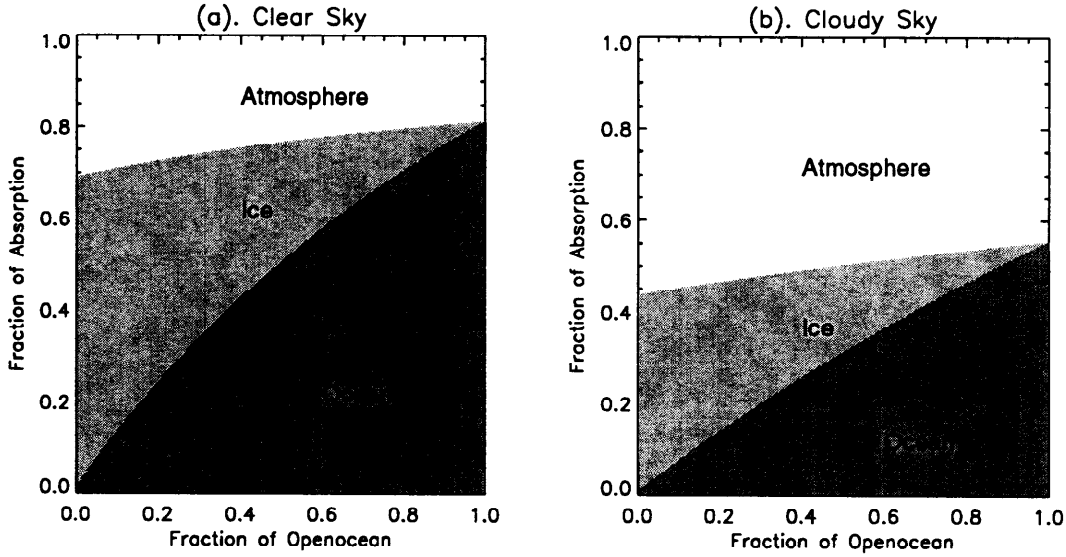

Figure 5. Distribution of the absorbed solar energy in the atmosphere, sea ice, and ocean as a function of open ocean fraction for (a) clear sky and (b) cloudy sky conditions.

under ice-free conditions for a clear sky. The increase of the absolute value is even more pronounced, because the total absorption in the entire system increases with the open water fraction. Although the fraction of total absorption both in the ice and in the ocean is sensitive to the open ocean fraction, especially under clear skies, the fraction deposited in the atmosphere is not.

3.6. Comparison With Observations

Desirable model-data comparisons require comprehensive optical data sets from the atmosphere, the ice, and the ocean. Unfortunately, such radiation measurements with simultaneous observational data on the environmental parameters required have, to date, not been made. This lack of data makes accurate comparisons with coupled radiative transfer models difficult. However, of all the radiation quantities, the spectral albedo of the ice surface is the only value on which the atmosphere and ocean have a minor influence if the sky is overcast (when the radiative incidence on the surface can be considered to be diffuse). In addition, only the properties of the thin top layer of the ice are important for this albedo, and so it is presently probably the best quantity available for comparison. Therefore we choose two observational spectral albedos for two relatively simple ice types. These are melting multiyear white ice and melting first-year blue ice. The observed spectral albedos are reproduced from the observations reported by *Grenfell and Maykut* [1977]. Unfortunately, the data needed to specify the model uniquely were not obtained, so the comparison is only approximate. In the computations, because melting ice is being considered, we have specified the average ice temperature as −2°C. For the multiyear ice considered in Figure 6, recently parameterized profiles of salinity and air volume developed by W. F. Weeks (unpublished field data from ice station Crystal, 1986) are used. The salinity is expressed as

$$S = 2.785Z + 1.984Z^4 \qquad (12a)$$

$$Z = z/h_i, \qquad 0 < Z \leq 1.0 \qquad (12b)$$

which is based on a total of 769 individual measurements from multiyear floes at which the actual ice thickness varied between 1.99 and 5.45 m. The Z in the formula is the normalized ice thickness, and z and h_i are the actual depth in ice and actual ice thickness, respectively. The air volume for the multiyear ice is parameterized as

$$V_a = 18.55 - 7.6Z + 257.1\exp(-46.3Z) \qquad (13)$$

In this simulation, air volume is used directly for model input, while the brine volume is calculated as discussed in section 2. For the first-year blue ice in Figure 7 we have used a salinity of 5‰ as in the tables above, a value representative of thick first-year ice, and a density of 0.94 Mg/m^3, which assumes that the air volume is negligible, as it usually is for the first-year blue ice. The comparisons shown in Figures 6 and 7 are in quite good agreement, particularly with respect to the wavelength dependence. For multiyear ice the model predicts a little higher albedo at shorter wavelengths and a little lower at longer wavelengths than observed. For the first-year ice the model predicts a little lower albedo overall. However, the agreement could be improved by adjusting one or more of the input parameters, for example, the salinity profile. At present, it is not possible to determine whether the differences between the model results and observations are the result of inaccurate representations of the ice properties and/or the inappropriately assumed parameters in the Mie calculations of the optical properties of the ice.

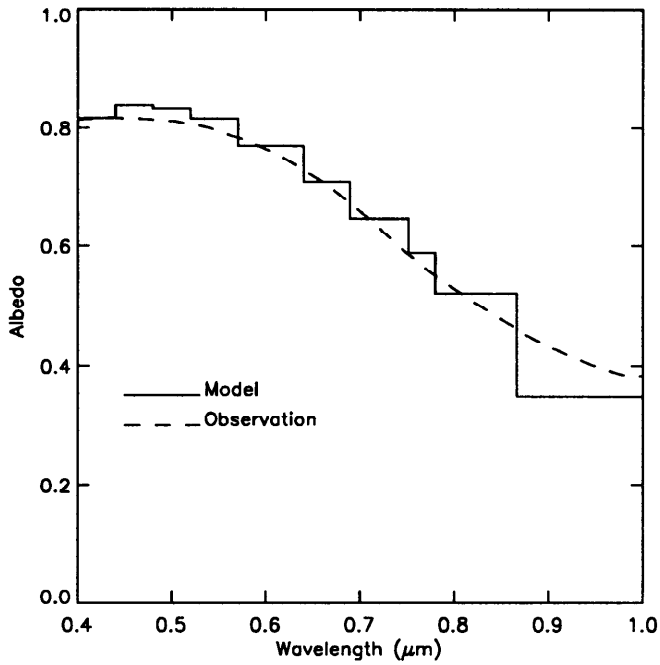

Figure 6. Comparison of observed spectral albedo for melting multiyear white ice with model calculations. Observations are from *Grenfell and Maykut* [1977].

4. Summary and Conclusions

The radiative energy budget in a coupled atmosphere, sea ice, and ocean system has been studied by using a newly developed radiative transfer model. In the atmosphere, gaseous absorption in 24 spectral bands spanning the entire solar spectrum has been implemented by a band model which allows for the inclusion of multiple scattering. Cloud effects have also been incorporated by parameterizing their optical properties. In sea ice the pure ice absorption, as well as the absorption and scattering by brine pockets and air bubbles, have been taken into account. The optical properties for the inclusions are based on Mie computations. In the ocean, absorption and scattering by seawater is considered. A snow layer on the ice is also included as an option. In addition, the refraction at the air-ice interface has been consistently taken into account.

The input parameters required by the model are observable physical properties (e.g., the profiles of temperature, pressure, and gas concentrations in the at-

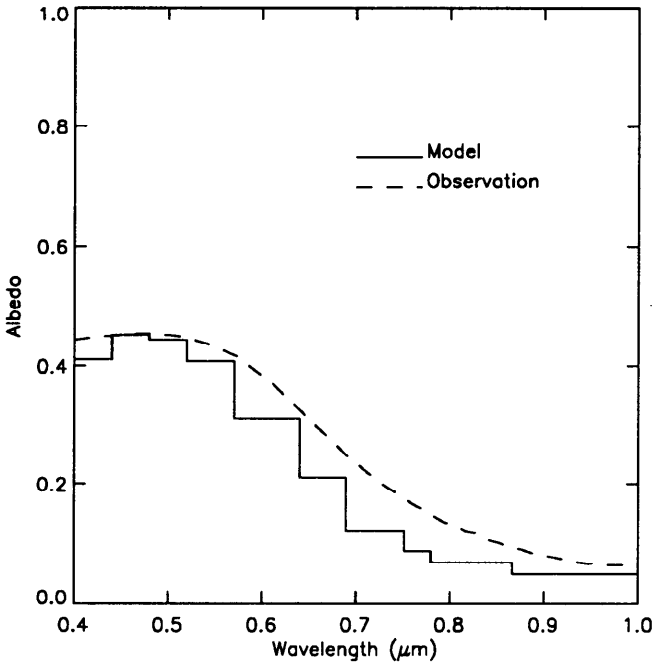

Figure 7. As in Figure 6, but for melting first-year blue ice.

mosphere, the water or ice content of clouds, and the equivalent radius of cloud droplets, as well as the profiles of temperature, density, and salinity in the ice).

This model has been applied to study the radiative interactions within the atmosphere, sea ice, and ocean system and to investigate the effects of the ice properties, ice thickness, snow, and cloud on the radiative energy disposition and its distribution within the coupled system. On the basis of the modeling results we can conclude that the sea ice has a significant impact on the absorption and partitioning of the solar radiative energy in the atmosphere, sea ice, and ocean system. Because changes in the physical properties of the ice, such as density, salinity, and temperature, lead to changes of the optical properties within the ice, such as scattering and absorption, and because of interactions occurring between the atmosphere, sea ice, and ocean, changes in the physical properties of the ice can alter the radiative transfer and the interaction processes within the entire system. Generally, as the ice density increases, the radiative absorption will increase in the entire coupled system, as well as in the sea ice and in the ocean, while the absorption in the atmosphere exhibits a slight decrease. As the ice salinity increases, the radiative absorption in the entire coupled system, in the ice, and in the ocean decreases. The absorption profiles in the ice show that most of the radiative energy absorbed by sea ice occurs in a very thin top layer of the ice. This is especially true under clear sky conditions. Only 10 cm of the top layer of ice can absorb more than 50% of the total solar radiation disposed in the entire system. Also, at depths greater than 50 cm in the ice, only visible radiation is left because of the strong absorption of the ice beyond this wavelength region.

In sea ice it is the scattering by inclusions, especially the air bubbles, in a few centimeters of the uppermost layer that plays the vital role to the solar energy absorption and partitioning in the whole system. Higher scattering in this top layer will not only increase backscattering to the atmosphere, but it also increases the absorption fraction in this top ice layer itself and decreases the radiation penetrating to the deeper layers of the ice and to the ocean. Because air bubbles have much higher scattering effectiveness than brine pockets, the radiative absorption is more sensitive to air volume variations than to brine volume variations. Therefore to estimate the solar energy distribution with confidence, one must be able to input realistic estimates of the air volume fraction in the ice. Estimates for the top few centimeters of the ice are particularly important.

Ice thickness also exerts a significant influence on the radiative energy balance in the atmosphere-sea ice-ocean system, especially when the ice is thin. Increasing the ice thickness in the thickness range between 0 and 70 cm results in an increase in the radiative absorption in the ice and a decrease in the ocean, as well as a decrease in the entire system. However, the total absorption in the entire system remains almost constant once the ice thickness exceeds about 70 cm. Nevertheless, the absorption within the atmosphere is not sensitive to the ice thickness change.

Clouds and snow on the ice reduce the solar energy absorption in the ice and in the ocean, as well as in the entire atmosphere-sea ice-ocean system. The main role of clouds seems to be to moderate any variation in the radiative energy budget caused by changes in ice properties and ice thickness. In other words, clouds reduce the sensitivity of the absorbed solar energy in every layer to changes in ice properties and thickness.

Realistic simulations of the radiative energy budget require in situ data from measurements. This includes the profiles of relevant parameters described above for the atmosphere, sea ice, and ocean, or else the profiles of optical properties, in particular, the light extinction and absorption, as well as the phase function of scattering. Simultaneous measurements of the radiative quantities, including the spectral upward and downward fluxes, would be very useful in verifying the model simulations.

We note that although our present treatment of the profile properties of the different thicknesses and ages of sea ice is crude and that we have assumed a linear temperature profile for all ice thicknesses, the model that has been described is capable of treating quite realistic property and temperature profiles. At the present we are attempting to develop improved parameterizations of sea ice property profiles for different ice types. Finally, we would like to state that the couplings that we have considered are purely radiative and do not allow the radiation to alter the snow/ice/cloud properties resulting in changes which could affect subsequent radiative transfer. In the future we hope to combine the coupled radiative transfer model with models treating the evolution of ice, snow, and clouds to investigate interactions and feedbacks in the polar climate.

Acknowledgments. The first author would like to thank Fé Semouer for help with writing the manuscript. This work was supported by the Department of Energy through contract 091574-A-Q1 to the University of Alaska.

References

Bennett, T. J., A coupled atmosphere-sea ice model study of the role of sea ice in climatic predictability, *J. Atmos. Sci., 39,* 1456-1465, 1982.

Buckley, R. G., and H. J. Trodahl, Scattering and absorption of visible light by sea ice, *Nature, 326,* 867-869, 1987.

Chandrasekhar, S., *Radiative Transfer*, Dover, Mineola, N. Y., 1960.

Coulson, K. L., *Solar and Terrestrial Radiation: Methods and Measurements*, 322 pp., Academic, San Diego, Calif., 1975.

Cox, G. F. N., and W. F. Weeks, Equations for determining the gas and brine volumes in sea ice samples, *J. Glaciol., 29,* 306-316, 1983.

Cox, G. F. N., and W. F. Weeks, Numerical simulations of the profile properties of underformed first-year sea ice during the growth season, *J. Geophys. Res., 93,* 12,449-12,460, 1988.

Ebert, E. E., and J. A. Curry, A intermediate one-dimensional thermodynamical sea ice model for investigating ice-atmosphere interactions, *J. Geophys. Res., 98,* 10,085-10,109, 1993.

Eicken, H., Salinity profiles of antarctic sea ice: Field data and model results, *J. Geophys. Res., 97,* 15,545-15,557, 1992.

Goody, R., and Y. L. Yung, *Atmospheric Radiation: Theoretical basis*, Oxford University Press, New York, 1989.

Grenfell, T. C., The effects of ice thickness on the exchange of solar radiation over the polar oceans, *J. Glaciol., 22,* 305-320, 1979.

Grenfell, T. C., A theoretical model of the optical properties of sea ice in the visible and near infrared, *J. Geophys. Res., 88,* 9723-9735, 1983.

Grenfell, T. C., A radiative transfer model for sea ice with vertical structure variations, *J. Geophys. Res., 96,* 16,991-17,002, 1991.

Grenfell, T. C., and G. A. Maykut, The optical properties of ice and snow in the Arctic basin, *J. Glaciol., 18,* 445-463, 1977.

Grenfell, T. C., and D. K. Perovich, Radiation absorption coefficients of polycrystalline ice from 400-1400 nm, *J. Geophys. Res., 86,* 7447-7450, 1981.

Herman, G. F., and J. Curry, Observational and theoretical studies of solar radiation in arctic stratus clouds, *J. Clim. Appl. Meteorol., 23,* 5-24, 1984.

Hunt, G. E., and I. P. Grant, Discrete space theory of radiative transfer and its application to problems in planetary atmospheres, *J. Atmos. Sci., 26,* 963-972, 1969.

Jin, Z., and K. Stamnes, Radiative transfer in nonuniformly refracting layered media: Atmosphere-ocean system, *Appl. Opt., 33,* 431-442, 1994.

Langleben, M. P., On the factors affecting the rate of ablation of sea ice, *Can. J. Earth Sci., 3,* 431-439, 1966.

Maykut, G. A., Energy exchange over young sea ice in the central Arctic, *J. Geophys. Res., 83,* 3646-3658, 1978.

Maykut, G. A., and T. C. Grenfell, The spectral distribution of light beneath first-year sea ice in the Arctic ocean, *Limnol. Oceanogr., 20,* 554-563, 1975.

Maykut, G. A., and N. Untersteiner, Some results from a time dependent thermodynamic model of sea ice, *J. Geophys. Res., 76,* 1550-1575, 1971.

McClatchey R. A., R. W. Fenn, J. E. A. Selby, F. E. Volz, and J. S. Garing, Optical properties of the atmosphere, *Rep. AFCRL-72-0497*, Air Force Cambridge Res. Lab., Bedford, Mass., 1972.

Morel, A. and R. C. Smith, Terminology and units in optical oceanography, *Mar. Geod., 5,* 335-349, 1982.

Parkinson C. L., and W. M. Washington, A large-scale numerical model of sea ice, *J. Geophys. Res., 84,* 311-337, 1979.

Perovich, D. K., Theoretical estimates of light reflection and transmission by spatially complex and temporally varying sea ice covers, *J. Geophys. Res., 95,* 9557-9567, 1990.

Perovich, D. K., and J. Gow, A statistical description of the microstructure of young sea ice, *J. Geophys. Res., 96,* 16,943-16,953, 1991.

Perovich, D. K., and G. A. Maykut, Solar heating of a stratified ocean in the presence of a static ice cover, *J. Geophys. Res., 95,* 18,233-18,245, 1990.

Rothman, L. S., et al., The HITRAN database: 1986 edition, *Appl. Opt., 26,* 4058-4097, 1987.

Semtner, A. J., A model for the thermodynamic growth of sea ice in numerical investigations of climate, *J. Phys. Oceanogr., 6,* 379-389, 1976.

Shine, K. P., and R. G. Crane, The sensitivity of a one-dimensional thermodynamic sea ice model to changes in cloudiness, *J. Geophys. Res., 89,* 10,615-10,622, 1984.

Slingo, A., A GCM parameterization for the shortwave radiative properties of water clouds, *J. Atmos. Sci., 46,* 1419-1427, 1989.

Smith, R. C., and K. S. Baker, Optical properties of the clearest natural waters, *Appl. Opt., 20,* 177-184, 1981.

Stamnes, K., The theory of multiple scattering of radiation in plane parallel atmospheres, *Rev. Geophys., 24,* 299-310, 1986.

Stamnes, K., and P. Conklin, A new multi-layer discrete ordinate approach to radiative transfer in vertically inhomogeneous atmospheres, *J. Quant. Spectrosc. Radiat. Transfer, 31,* 273-282, 1984.

Stamnes, K., S. C. Tsay, W. J. Wiscombe, and K. Jayaweera, Numerically stable algorithm for discrete-ordinate-method radiative transfer in multiple scattering and emitting layered media, *Appl. Opt., 27,* 2502-2509, 1988.

Tsay S. C., and K. Jayaweera, Physical characteristics of Arctic stratus clouds, *J. Clim. Appl. Meteorol., 23,* 584-596, 1984.

Tsay, S. C., K. Stamnes, and K. Jayaweera, Radiative energy budget in the cloudy and hazy Arctic, *J. Atmos. Sci., 46,* 1002-1018, 1989.

Untersteiner, N., On the mass and heat budget of arctic sea ice, *Arch. Meteorol. Geophys. Bioklimatol., Ser. A, 12,* 151-182, 1961.

Van Ypersele, J.-P., Modeling sea ice for climate studies, in *Climate-Ocean Interaction*, edited by M. E. Schlesinger, pp. 97-123, Kluwer Academic Publ., Dordrecht, Netherlands, 1990.

Warren, S. G., Optical constants of ice from the ultraviolet to the microwave, *Appl. Opt., 23,* 1206-1225, 1984.

Warren S. G., and W. J. Wiscombe, A model for the spectral albedos of snow, 2, Snow containing atmospheric aerosols, *J. Atmos. Sci., 37,* 2734-2745, 1980.

Wiscombe, W. J., and J. W. Evans, Exponential-sum fitting of radiative transmission functions, *J. Comput. Phys., 24,* 416-444, 1977.

Wiscombe, W. J., and S. G. Warren, A model for the spectral albedos of snow, 1, Pure snow, *J. Atmos. Sci., 37,* 2712-2733, 1980.

Z. Jin, K. Stamnes and W. F. Weeks, Geophysical Institute, University of Alaska, 903 Koyukuk Drive, P. O. Box 757320, Fairbanks, AK 99775.

S.-C. Tsay, NASA Goddard Space Flight Center, Code 913, Greenbelt, MD 20771.

(Received January 10, 1994; revised August 17, 1994; accepted September 9, 1994.)